Syntheses, Structural Analyses, and Unusual Magnetic Properties of $Ba_2CoSi_2O_7$ and $BaCo_2Si_2O_7$

Richard D. Adams* and Ralph Layland

Department of Chemistry and Biochemistry, University of South Carolina, Columbia, South Carolina 29208

Christophe Payen*

Institut des Matériaux de Nantes, 2 rue de la Houssinière, 44072 Nantes Cedex 03, France

Timir Datta

Department of Physics, University of South Carolina, Columbia, South Carolina 29208

Received February 15, 1996[⊗]

The compounds $Ba_2CoSi_2O_7$, **1**, and $BaCo_2Si_2O_7$, **2**, were obtained by heating mixtures of $BaCO_3$, $CoCO_3$, and SiO_2 in the proper stoichiometries to 1300 °C for 48 h. Both materials were characterized by single-crystal X-ray diffraction and magnetization measurements on powder and partially oriented single crystals. Each cobalt ion in **1** is surrounded by four oxygen atoms derived from the $[Si_2O_7]^{6-}$ groups in the form of a distorted tetrahedron. The cobalt ions are bridged by O−Si−O and O−Si−O−Si−O groups from the $[Si_2O_7]^{6-}$ ions in an extended two-dimensional arrangement. The barium ions are arranged in layers that run parallel to the $Co[Si_2O_7]$ layers. In **2** each cobalt ion is also surrounded by an arrangement of four oxygen atoms derived from the Si_2O_7 groups in a distorted tetrahedral shape. These tetrahedra are linked into chains through the sharing of one of the oxygen atoms from the Si_2O_7 groups. The CoO_4 chains are crosslinked via O−Si−O−Si−O bridges from the Si_2O_7 groups. The barium ions occupy channels that run parallel to the crystallographic *c*-axis. Curie−Weiss behaviors and temperature independent paramagnetisms (TIP) coexist in the ranges 40−300 K and 100−300 K for **1** and **2**, respectively. For both compounds the values of the Curie constant and TIP are consistent with tetrahedral Co(II) ions having three unpaired electrons. While compound **1** remains paramagnetic down to 5 K, **2** undergoes a transition into a state having a field-induced weak ferromagnetic response at $T_c = 21$ K. The weak ferromagnetic properties below T_c can be explained by spin canting and spontaneous domain formation. The canting angle is estimated to be about 5° at 5 K. Interestingly, **2** could represent the first example among the tetrahedral Co(II) compounds with the transition temperature ($T_c = 21$ K) being higher than the zero-field splitting of the $^4A_2$ electronic ground state. Crystal data: for **1**, formula $Ba_2CoSi_2O_7$, $a = 8.450(1)$ Å, $b = 10.729(1)$ Å, $c = 8.474(1)$ Å, $\beta = 111.365(8)°$, monoclinic, space group = $C2/c$, $Z = 4$; for **2**, formula $BaCo_2Si_2O_7$, $a = 7.2131(6)$ Å, $b = 12.781(1)$ Å, $c = 13.762(1)$ Å, $\beta = 90.299(8)°$, monoclinic, space group = $C2/c$, $Z = 8$.

Low-dimensional materials exhibiting anisotropic transport and unusual magnetic properties have been the source of great interest.[1] Efforts to synthesize these materials have recently attracted considerable attention.[2] Silicates are well-known for their ability to form two-dimensional layered structures.[3] Many mixed alkaline earth/transition metal silicates with the general formula $M_2M'Si_2O_7$, M = alkaline earth and M′ = transition metal, crystallize in a layered structural form characteristic of minerals known as akermanites (e.g. $Ca_2MgSi_2O_7$).[4] The low-dimensional character of the materials can be enhanced by the presence of the large ions such as barium. In this report the preparation, structural characterization, and magnetic properties of the compounds $Ba_2CoSi_2O_7$, **1**, and $BaCo_2Si_2O_7$, **2**, are described. Compound **1** contains a two-dimensional lattice, while compound **2** exhibits a novel one-dimensional pattern formed by chains of CoO_4 tetrahedra.[5] Magnetic studies were originally undertaken to find out if **2** possesses any 1D magnetic properties that might be derived from the cobalt chains embedded in a diamagnetic matrix. The results indicate that the signatures of 1D antiferromagnetic fluctuations are, in fact,

[⊗] Abstract published in *Advance ACS Abstracts,* May 15, 1996.

(1) (a) Day, P. In *Solid State Chemistry Compounds*; Cheetham, A. K., Day, P., Eds.; Clarendon Press: Oxford, U.K., 1992; Chapter 2. (b) Rao, C. N. R.; Ganguli, A. K. *Chem. Soc. Rev.* **1995**, 1. (c) Miller, J. S.; Epstein, A. J. *Prog. Inorg. Chem.* **1994**, *33*, 385. (d) Schlenker, C.; Dumas, J. *Crystal Chemistry and Properties of Materials with Quasi-One-Dimensional Structures. A Chemical and Physical Synthetic Approach;* Rouxel, J., Ed.; D. Reidel Publishing Co.: Dordrecht/Boston/Lancaster/Tokyo, 1986; p 135. (e) Metzger, R. M., Day, P., Papavassiliou, G. C., Eds. *Lower-Dimensional Systems and Molecular Electronics*; Plenum: New York, 1990. (f) Cava, R. J. *Science* **1990**, *247*, 656. (g) Poole, C. P., Jr.; Datta, T.; Farach, H. A. *J. Superconduct.* **1989**, *2*, 369. (h) Greenblatt, M. *Chem. Rev.* **1988**, *88*, 31.

(2) (a) Simon, A. *Angew. Chem., Int. Ed. Engl.* **1988**, *27*, 159. (b) Corbett, J. D. In *Perspectives in Coordination Chemistry;* Williams, A. F., Floriani, C. F., Merbach, A. E., Eds.; VCH Publishers: Weinheim, Germany, 1992; p 219. (c) Ziebarth, R. P.; Corbett, J. D. *Acc. Chem. Res.* **1989**, *22*, 256. (d) Corbett, J. D. *Pure Appl. Chem.* **1984**, *56*, 1527. (e) Meyer, G. *Chem. Rev.* **1988**, *88*, 93.

(3) (a) Griffen, D. T. *Silicate Crystal Chemistry*; Oxford University Press: New York, 1992. (b) Liebau, F. *Structural Chemistry of Silicates*; Springer-Verlag: Berlin, 1985.

(4) (a) Ito, J.; Peiser, H. S. *J. Res (NBS)* **1969**, *73A*, 69. (b) Finch, C. B.; Clark, G. W.; Harris, L. A.; Yust, C. S. *J. Cryst. Growth* **1974**, *23*, 295. (c) Ii, N.; Shindo, I. *J. Cryst. Growth* **1979**, *46*, 569. (d) Kimata, M. *Z. Kristallogr.* **1983**, *163*, 295.

(5) Adams, R. D.; Layland, R.; Datta, T.; Payen, C. *Polyhedron* **1993**, *12*, 2075.

S0020-1669(96)00167-X CCC: $12.00

Table 1. Crystallographic Data for Compounds **1** and **2**

	compound	
	1	**2**
formula	$Ba_2CoSi_2O_7$	$BaCo_2Si_2O_7$
fw	501.76	423.36
a (Å)	8.450(1)	7.2131(6)
b (Å)	10.729(1)	12.781(1)
c (Å)	8.474(1)	13.762(1)
β (deg)	111.365(8)	90.299(8)
V (Å^3)	715.4(3)	1268.7(3)
space group	$C2/c$ (No. 15)	$C2/c$ (No. 15)
Z	4	8
temp (°C)	20	20
λ (Mo) Å	0.710 69	0.710 69
ρ_{calc} (g/cm^3)	4.66	4.43
μ(Mo Kα) (cm^{-1})	135.1	116.7
R^a	0.021	0.042
$R_w{}^a$	0.026	0.056

[a] $R = \sum_{hkl}(||F_o| - |F_c||/\sum_{hkl}|F_o|$; $R_w = [\sum_{hkl}w(|F_o| - |F_c|^2)/\sum_{hkl}wF_o{}^2]^{1/2}$, $w = 1/\sigma^2(F_o)$.

probably masked by a spin-canting phenomenon that leads to a weak ferromagnetic state below $T_c = 21$ K. Compound **2** provides, however, a very interesting system in the magnetochemistry of tetrahedral Co(II). In particular, **2** could represent the first example with the transition temperature ($T_c = 21$ K) being higher than the zero-field splitting of the $^4A_2$ electronic ground state.

Experimental Section

$BaCO_3$ (98%), SiO_2 (99.99%), and $CoCO_3$ (99.9%) were purchased from Aldrich and were used without further purification. The mixtures were heated in a Lindberg Model 51333 furnace. X-ray powder diffraction measurements were performed on a Rigaku powder diffractometer using Cu Kα radiation ($\lambda = 1.5418$ Å).

Preparation of $Ba_2CoSi_2O_7$. A mixture of 0.7903 g (4.01 mmol) of $BaCO_3$, 0.2376 g (2.00 mmol) of $CoCO_3$, and 0.2409 g (4.00 mmol) of SiO_2 was ground thoroughly in a mortar and then transferred into a platinum crucible. The platinum crucible was placed in the furnace and heated in air to 1300 °C for 48 h. After this period, the furnace was cooled slowly (approximately 1 °C/min) to 900 °C and then allowed to cool rapidly to 500 °C. At room temperature the sample was removed from the oven.

Preparation of $BaCo_2Si_2O_7$. A mixture of 0.789 g (4.00 mmol) of $BaCO_3$, 0.9515 g (8.00 mmol) of $CoCO_3$, and 0.4816 g (8.01 mmol) of SiO_2 was ground thoroughly in a mortar and then transferred to a platinum crucible. The crucible was placed in the oven and heated in air to 1300 °C for 48 h. After this period, the oven was cooled slowly (approximately 1 °C/min.) to 1000 °C and then allowed to cool quickly to 500 °C. At this temperature the sample was removed from the oven. An X-ray powder analysis of **2** showed that some samples contained traces of CoO and $BaCoSiO_4$.

Crystallographic Analyses. Royal blue crystals of **1** and **2** were cleaved from the appropriate bulk samples. Diffraction measurements at 20 °C were made on a Rigaku AFC6S four-circle diffractometer. The unit cells were determined from 15 randomly selected reflections. Crystal data, data collection parameters, and results of the analyses are listed in Table 1. All calculations were performed on a Digital Equipment Corp. VAXstation 3520 computer by using the TEXSAN structure-solving program library obtained from the Molecular Structure Corp., The Woodlands, TX. Neutral atom scattering factors were calculated by the standard procedures.[6a] Anomalous dispersion corrections were applied to all non-hydrogen atoms.[6b] Full-matrix least-squares refinements minimized the function: $\sum_{hkl}w(|F_o| - |F_c|)^2$, where $w = 1/\sigma(F)^2$, $\sigma(F) = \sigma(F_o{}^2)/2F_o$, and $\sigma(F_o{}^2) = [\sigma(I_{raw})^2 + (0.02I_{net})^2]^{1/2}/Lp$.

Both compounds crystallized in the monoclinic crystal system. The patterns of systematic absences observed in the data were consistent with either of the space groups Cc or $C2/c$. The centric space group $C2/c$ was assumed and confirmed by the successful solution and refinement of the structures in each case. The structures were solved by a combination of direct methods (MITHRIL) and difference Fourier syntheses. All atoms were refined with anisotropic thermal parameters.

Table 2. Positional Parameters and B(eq) Values (Å^2) for $Ba_2CoSi_2O_7$, **1**

atom	x	y	z	B(eq)[a]
Ba	1.27393(04)	0.45776(03)	0.02623(04)	0.69(2)
Co	1.0000	0.25820(11)	1/4	0.70(4)
Si	0.8862(02)	0.28250(16)	−0.1380(02)	0.58(6)
O(1)	1.0000	0.3329(06)	−1/4	1.2(2)
O(2)	0.6998(05)	0.3436(04)	−0.2360(05)	0.8(1)
O(3)	0.9727(05)	0.3525(04)	0.0432(05)	0.9(2)
O(4)	0.8907(05)	0.1324(04)	−0.1322(05)	0.9(2)

[a] $B(\text{eq}) = 8\pi^2/3\sum_{i=1}^{3}\sum_{j=1}^{3}U_{ij}a_i^*a_j^*\vec{a}_i\vec{a}_j$. See: Fischer, R. X.; Tillmanns, E. *Acta Crystallogr.* **1988**, *C44*, 775.

Table 3. Positional Parameters and B(eq) Values (Å^2) for $BaCo_2Si_2O_7$, **2**

atom	x	y	z	B(eq)[a]
Ba	0.19603(06)	0.01940(04)	0.12214(03)	0.57(2)
Co(1)	1/2	0.27175(12)	1/4	0.58(5)
Co(2)	1/2	−0.26949(12)	1/4	0.58(5)
Co(3)	0.03207(14)	0.23010(08)	0.51050(07)	0.43(4)
Si(1)	0.2908(03)	−0.12326(16)	0.36633(15)	0.37(7)
Si(2)	0.3233(03)	0.10557(16)	0.38086(14)	0.35(7)
O(1)	0.4279(08)	−0.2218(04)	0.3856(04)	0.7(2)
O(2)	0.1703(08)	0.1154(04)	0.2963(04)	0.8(2)
O(3)	0.2481(07)	0.1347(04)	0.4880(04)	0.6(2)
O(4)	0.5038(07)	0.1818(04)	0.3670(04)	0.5(2)
O(5)	0.4138(08)	−0.0130(04)	0.3782(04)	0.6(2)
O(6)	0.2213(08)	−0.1366(04)	0.2543(04)	1.0(2)
O(7)	0.1251(08)	−0.1112(04)	0.4439(04)	0.7(2)

[a] See footnote *a* of Table 2.

Magnetic Measurements. Dc magnetic measurements were performed on a Quantum Design MPMS SQUID magnetometer at temperatures ranging from 5 to 300 K. All data were first corrected for the effects of the sample holder and then for ionic diamagnetism using the values $\chi_{dia} = -147 \times 10^{-6}$ emu/mol and -67×10^{-6} emu/Co mol for **1** and **2**, respectively.[7] To ensure purity, samples were obtained by using carefully hand-selected material. Both compounds exhibited a strong preference for platelike crystalline habits. A 149.3 mg amount of **1** and 41.9 mg of **2** having random crystal orientations were used in the measurements, but measurements of **2** were also performed on partially oriented single crystals (typically 5−10 crystals in the form of well-shaped platelets) with the magnetic field applied parallel to the crystallographic b-axis and also parallel to the crystallographic ac-plane. It was assumed that all crystals had the same crystallographic orientation as the one analyzed by single-crystal X-ray diffraction. Ac susceptibility measurements were made on a Lakeshore susceptometer operating at a frequency of 600 Hz and an alternating field $H = 10$ Oe. A 41.0 mg amount of randomly oriented crystals was used for the measurements of **2**.

Results and Discussion

$Ba_2CoSi_2O_7$, **1**, was obtained from the reaction of a 2/1 mixture of $BaCO_3$ and $CoCO_3$ with SiO_2 by heating in a platinum crucible to 1300 °C for 48 h. A compound of similar formula was reportedly obtained from the reaction $BaCO_3$, Co_3O_4, and silicic acid by heating to 1200 °C.[8] We have performed a full three-dimensional single-crystal structural analysis of **1** which is reported here. The final crystallographic positional parameters for the analysis of **1** are listed in Table 2. A projection of the crystallographic unit cell perpendicular to the ac plane is shown in Figure 1. Selected bond distances

(6) (a) *International Tables for X-ray Crystallography*; Kynoch Press: Birmingham, England, 1975; Vol. IV, Table 2.2B, pp 99−101. (b) *Ibid.*, Table 2.3.1, pp 149−150.

(7) Mulay, L. N.; Boudreaux, E. A. *Theory and Application of Molecular Diamagnetism*; Wiley-Interscience: New York, 1976.

(8) Brisi, C.; Abbattista, F. *Ann. Chim.* **1960**, *50*, 1435.

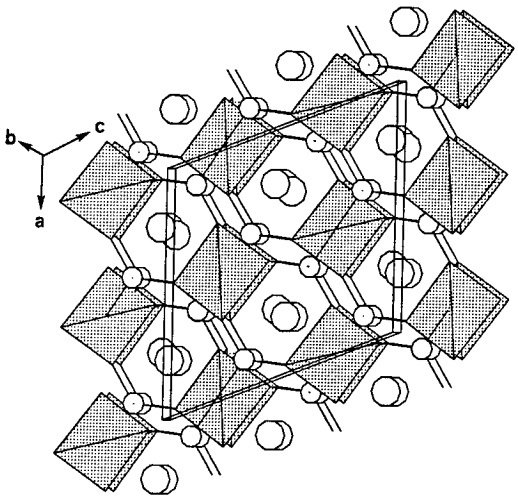

Figure 1. Projection of the solid-state structure of $Ba_2CoSi_2O_7$, **1**, in the *ac*-plane showing the arrangement of CoO_4 tetrahedra. CoO_4 tetrahedra are represented by the shaded polyhedra. Bonds between the silicon atoms (small circles) and oxygen atoms are shown, but the oxygen atoms are not drawn. The connectivities of the barium atoms (large circles) are not shown.

Table 4. Intramolecular Bond Distances and Angles for **1**[a]

	Distances		
Ba−O(1)	2.947(3)	Ba−Ba′	4.2921(9)
Ba−O(2)	2.828(4)	Ba−Ba″	4.1055(9)
Ba−O(2′)	2.732(4)	Co−O(2)	1.978(4)
Ba−O(3)	2.836(4)	Co−O(3)	1.963(4)
Ba−O(3′)	2.818(4)	Si−O(1)	1.668(3)
Ba−O(4)	2.693(4)	Si−O(2)	1.628(4)
Ba−O(4′)	2.864(4)	Si−O(3)	1.624(4)
Ba−O(4″)	2.814(4)	Si−O(4)	1.611(5)
	Angles		
O(3)−Co−O(3′)	117.9(3)	O(1)−Si−O(3)	103.5(2)
O(2)−Co−O(2′)	112.9(3)	O(1)−Si−O(4)	109.2(3)
O(2)−Co−O(3)	99.1(2)	O(2)−Si−O(3)	108.3(2)
O(2)−Co−O(3′)	114.3(2)	O(2)−Si−O(4)	115.2(2)
O(1)−Si−O(2)	103.3(2)	O(3)−Si−O(4)	115.9(2)

[a] Distances are in Å, angles are in deg. Estimated standard deviations in the least significant figure are given in parentheses.

and angles are listed in Table 4. Each cobalt ion is surrounded by a distorted tetrahedral arrangement of four oxygen atoms that are derived from the $[Si_2O_7]^{6-}$ groups, Co−O = 1.963(4) and 1.978(4) Å. These values are similar to those in other silicate coordinated CoO_4 tetrahedra.[9] These arrangements are represented by the tetrahedral shapes shown in the figure. The cobalt ions and $[Si_2O_7]^{6-}$ groups are arranged into a two-dimensional extended layer via O−Si−O and O−Si−O−Si−O bridging linkages of the $[Si_2O_7]^{6-}$ groups. The barium ions are arranged in layers that run parallel to the $Co[Si_2O_7]$ layers and the crystallographic *ac*-plane. This can be seen in the projection of the crystallographic *ab*-plane that is shown in Figure 2. The structure of $Ba_2CoSi_2O_7$ is isomorphous to the previously reported compound $Ba_2CuSi_2O_7$.[10,11]

$BaCo_2Si_2O_7$, **2**, was obtained by heating a 1/2 mixture of $BaCO_3$ and $CoCO_3$ with SiO_2 to 1300 °C for 48 h. Its three-dimensional structure was established by a single-crystal X-ray diffraction analysis, and a projection of the crystallographic unit

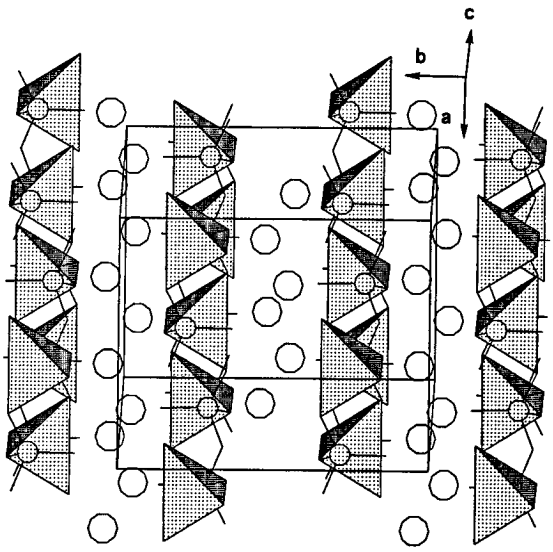

Figure 2. Projection of the solid-state structure of $Ba_2CoSi_2O_7$, **2**, in the *ab*-plane showing the layers of CoO_4 tetrahedra and barium ions running parallel to the *ac* plane. CoO_4 tetrahedra are represented by the shaded polyhedra. Bonds between the silicon atoms (small circles) and oxygen atoms are shown, but the oxygen atoms are not drawn. The connectivities of the barium atoms (large circles) are not shown.

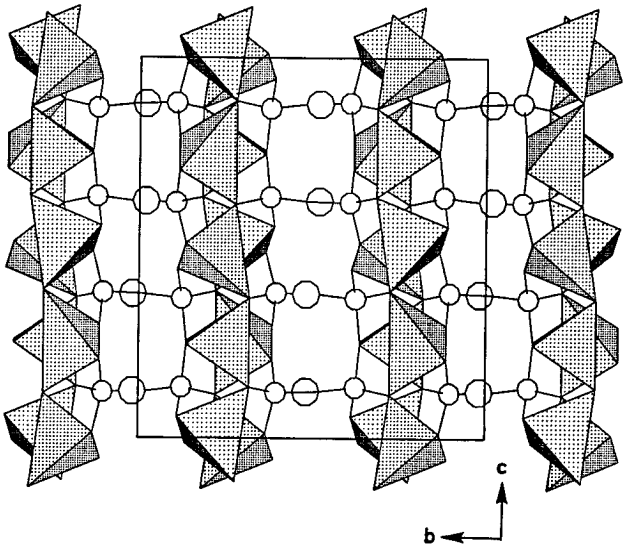

Figure 3. Projection of the solid-state structure of $BaCo_2Si_2O_7$ in the *bc*-plane showing the chains of CoO_4 tetrahedra running parallel to the *c*-axis. CoO_4 tetrahedra are represented by the shaded polyhedra. Bonds between the silicon (small circles) and oxygen atoms are shown, but the oxygen atoms are not drawn. The connectivities of the barium atoms (large circles) are not shown.

cell perpendicular to the *bc*-plane is shown in Figure 3. The final crystallographic positional parameters for the analysis of **2** are listed in Table 3. Selected bond distances and angles are listed in Tables 5 and 6. As in **1**, each cobalt ion is surrounded by a distorted tetrahedral arrangement of four oxygen atoms derived from the $[Si_2O_7]^{6-}$ groups. The tetrahedra are linked into a novel arrangement of chains through the mutual sharing of one of the oxygen atoms, Co−O = 1.971(6)−2.045(5) Å.[9] The CoO_4 chains are crosslinked via O−Si−O bridges of the Si_2O_7 groups in the *a*-direction and via O−Si−O−Si−O bridges in the *b*-direction. The barium ions lie in channels that run parallel to the *c*-crystallographic axis. The compound $BaCoSiO_4$, **3**, was reportedly obtained from appropriate mixtures of barium acetate, cobalt carbonate, and silica gel combined at high temperature,[12] and small amounts of **3** were found in some of our preparations of **1** and **2**.

(9) (a) Kimata, M. *Naturwissenschaften* **1982**, *69*, 40. (b) Yamaguchi, H.; Akatsuka, K.; Setoguchi, M.; Takaki, Y. *Acta Crystallogr.* **1979**, *B35*, 2680.

(10) Malinovskii, Yu. A. *Sov. Phys. Dokl.* **1984**, *29*, 706.

(11) It was reported that $Ba_2CuSi_2O_7$ crystallizes in the monoclinic crystal system in the space group *A*2/*a*.[7] The setting may have been misstated since the reported lattice parameters appear to represent a *B*-setting that would correspond to our *C*-setting for $Ba_2CoSi_2O_7$ after a suitable transformation.

Table 5. Interatomic Distances for $BaCo_2Si_2O_7$, **2**[a]

Ba−O(2)	2.706(5)	Co(3)−O(1)	1.971(6)
Ba−O(2)	3.132(6)	Co(3)−O(3)	2.004(5)
Ba−O(3)	2.718(5)	Co(3)−O(4)	2.045(5)
Ba−O(4)	3.011(5)	Co(3)−O(7)	1.999(5)
Ba−O(5)	2.843(6)	Si(1)−O(1)	1.622(6)
Ba−O(6)	2.695(6)	Si(1)−O(5)	1.673(6)
Ba−O(7)	2.985(6)	Si(1)−O(6)	1.627(6)
Ba−O(7)	2.771(6)	Si(1)−O(7)	1.614(5)
Co(1)−O(4)	1.979(5)	Si(2)−O(2)	1.604(6)
Co(1)−O(6)	1.981(6)	Si(2)−O(3)	1.617(5)
Co(2)−O(1)	2.033(5)	Si(2)−O(4)	1.638(6)
Co(2)−O(2)	2.018(6)	Si(2)−O(5)	1.650(5)

[a] Distances are in Å. Estimated standard deviations in the least significant figure are given in parentheses.

Table 6. Interatomic Bond Angles for **2**[a]

O(4)−Co(1)−O(4′)	108.9(3)	O(3)−Co(3)−O(4)	124.4(2)
O(4)−Co(1)−O(6)	108.1(2)	O(7)−Si(1)−O(1)	114.8(3)
O(4)−Co(1)−O(6′)	112.1(2)	O(7)−Si(1)−O(6)	114.2(3)
O(6)−Co(1)−O(6′)	107.5(4)	O(7)−Si(1)−O(5)	104.4(3)
O(2)−Co(2)−O(2′)	86.4(3)	O(1)−Si(1)−O(6)	104.9(3)
O(2)−Co(2)−O(1)	95.0(2)	O(1)−Si(1)−O(5)	108.4(3)
O(2)−Co(2)−O(1′)	110.5(2)	O(6)−Si(1)−O(5)	110.0(3)
O(1)−Co(2)−O(1′)	145.1(3)	O(2)−Si(2)−O(3)	114.2(3)
O(1)−Co(3)−O(7)	107.3(2)	O(2)−Si(2)−O(4)	114.4(3)
O(1)−Co(3)−O(3)	110.4(2)	O(2)−Si(2)−O(5)	109.1(3)
O(1)−Co(3)−O(4)	119.8(2)	O(3)−Si(2)−O(4)	103.9(3)
O(7)−Co(3)−O(3)	91.6(2)	O(3)−Si(2)−O(5)	111.5(3)
O(7)−Co(3)−O(4)	94.9(2)	O(4)−Si(2)−O(5)	103.2(3)

[a] Angles are in deg. Estimated standard deviations in the least significant figure are given in parentheses.

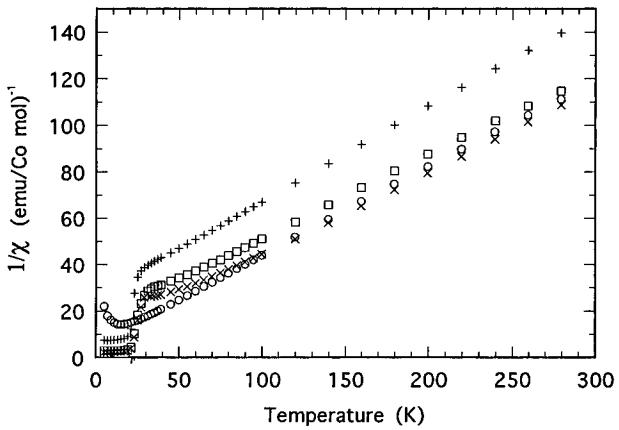

Figure 4. Plots of the inverse dc magnetic susceptibilities obtained at $H = 5$ kOe in the range 5−300 K on powders of $Ba_2CoSi_2O_7$ (○) and $BaCo_2Si_2O_7$ (□) and on partially oriented single crystals of $BaCo_2Si_2O_7$ for H parallel to the b-axis (+) or to the ac-plane (×).

Figure 4 shows the inverse dc magnetic susceptibilities obtained on samples of **1** and **2** between 5 and 300 K. In this figure, the susceptibility has been defined as the ratio of the magnetization M to the applied field H ($\chi = M/H$). All data were obtained on warming in $H = 5$ kOe, after the samples had been cooled in a zero field to 5 K. In the high temperature (T) range, the quasi-linear dependences of $1/\chi$ vs T prompted us to fit each susceptibility to a modified Curie−Weiss expression, $\chi(T) = C/(T - \Theta) + \chi_0$, where χ_0 allows for temperature-independent paramagnetism (TIP). The occurence of TIP was suspected from slight curvatures in the $1/\chi$ plots (Figure 4). Table 7 lists the values of C, Θ and χ_0 obtained from fits by least squares between 120 and 300 K. The magnetic moments $\mu = (8C)^{1/2}$ lie in the range 4.1−4.7 μ_B, and this is expected for a Co(II) ion in a tetrahedral environment with three

Table 7. Paramagnetic Parameters Obtained from Fits to $\chi(T) = C/(T - \Theta) + \chi_0$ between 120 and 300 K for $Ba_2CoSi_2O_7$, **1** (Powder), and for $BaCo_2Si_2O_7$, **2** (Powder and Partially Oriented Single Crystals)[a]

	1	**2**		
			partially oriented crystals	
	powder	powder	$H\|\|b$	$H\|\|ac$
C (emu·K·(mol of Co)$^{-1}$)	2.33(4)	2.25(6)	2.11(3)	2.76(1)
Θ (K)	−6(1)	−21(3)	−48(1)	−30(2)
χ_0(emu·(mol of Co)$^{-1}$)	0.0008(1)	0.0012(1)	0.0007(1)	0.0006(1)
$\mu = (8C)^{1/2}$ (μ_B)	4.3	4.2	4.1	4.7

[a] The values in parentheses are standard deviations of the least-squares fit.

unpaired electrons.[13,14] An isolated ion such as this has a formal $^4A_2$ ground state, and the formula for its susceptibility is

$$\chi = \mu^2/3kT + 8\mu B^2/10Dq \qquad (1)$$

where all the parameters have their usual meaning.[15] Spin−orbit coupling, which introduces an orbital contribution into the initially orbitally nondegenerate ground term, should lead to magnetic moments greater than the spin only value, 3.9 μ_B.[15] Indeed, experimental moments for tetrahedral high-spin Co(II) lie mostly in the range 4.0−4.8 μ_B.[13,14] Futhermore, the TIP term of $8\mu B^2/10Dq$ in eq 1 can be estimated from the experimental crystal-field-splitting parameters $10Dq$ that lie in the range 2700−5100 cm^{-1} [14] and from the free ion spin−orbit constant $\lambda = -178$ cm^{-1}.[16] Substituting these values gives TIP contributions lying in the range 4×10^{-4}−8×10^{-4} emu/mol of Co. Our experimental values are indeed on the same order of magnitude (see Table 7).

Since the local ground states for both compounds are not orbitally degenerate, it is tempting to interpret the negative Θ temperatures (Table 7) in terms of short-range antiferromagnetic interactions. However, zero-field splitting (ZFS) of the $^4A_2$ ground terms by the actual distortions from regular tetrahedral environments about Co(II) may introduce significant contributions to the Θ temperatures. Departures of the magnetic behavior of Co(II) ions from the simple Curie law have been attributed both to antiferromagnetic interactions and ZFS of the $^4A_2$ ground term.[14,17,18] In the simple case of an axial crystalline field acting on an isolated CoX_4 tetrahedron, it can be easily verified that ZFS causes a departure from Curie law. This departure can be treated empirically by means of the Curie−Weiss law with a Θ temperature on the same order as the ZFS parameter D, but this Θ temperature has no relationship with the Weiss constant of the molecular field approximation. Since for compounds of tetrahedral Co(II) the ZFS values are quite large, on the order of 10−15 K,[18,19] it is thus not possible to conclude that the small $\Theta = -6(1)$ K in **1** is due to the occurrence of significant antiferromagnetic interactions. In contrast, the larger Θ temperatures for **2** (Table 7) suggest the existence of contributions both from significant superexchange (antiferromagnetic) interactions as well as ZFS. The single-ion anisotropy induced by ZFS is indeed seen in the noticeable

(12) Liu, B.; Barbier, J. *J. Solid State Chem.* **1993**, *102*, 115.
(13) Banci, L.; Bencini, A.; Benelli, C.; Gatteschi, D.; Zanchini, C. *Struct. Bonding* **1982**, *52*, 37.
(14) Carlin, R. L. *Transition Metal Chemistry;* Marcel Dekker, Inc.: New York, 1965; Vol. 1.
(15) Mabbs, F. E.; Machin, D. J. *Magnetism and Transition Metal Complexes*; Chapman and Hall: London, 1973.
(16) Abragam, A.; Bleaney, B. *Electron Paramagnetic Resonance of Transition Ions*; The Clarendon Press: Oxford, U.K., 1969.
(17) Figgis, B. N. *Trans. Faraday Soc.* **1960**, *56*, 1553.
(18) Carlin, R. L. *Magnetochemistry*; Springer-Verlag: Berlin, 1986.
(19) Carlin, R. L. *Science* **1985**, *227*, 1291.

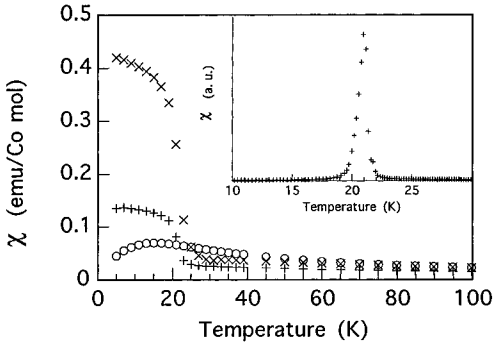

Figure 5. Plots of the dc magnetic susceptibilites for a powder of $Ba_2CoSi_2O_7$ (○) and for partially oriented single crystals of $BaCo_2Si_2O_7$ for *H* parallel to the *b*-axis (+) or to the *ac*-plane (×), over the range 5−100 K. The insert shows a plot of the in-phase ac susceptibility obtained at 10 Oe and $f = 600$ Hz on a powder sample of $BaCo_2Si_2O_7$.

paramagnetic anisotropy observed in the measurements of the oriented single crystals (Figure 4 and Table 7). Magnetic anisotropies on the same order of magnitude have been observed in other compounds of distorted tetrahedral Co(II) ions, and they have been explained in ZFS terms.[20]

Departures from the paramagnetic behaviors described above are observed with decreasing temperatures. This can be seen in Figures 4 and 5. The latter shows the dc χ vs T curves between 5 and 100 K. For **1**, the deviation from empirical Curie−Weiss behavior begins at about 40 K, and a susceptibility maximum occurs around 15 K. Apparently, this maximum does not precede the onset of long-range antiferromagnetic order since there are no peaks down to 5 K in either the $d\chi/dT$ vs T or the Fisher's specific heat $d(\chi T)/dT$ vs T curves. Zeeman energies being negligible, ZFS may once again be entirely responsible for this low-T behavior because the thermal energy available at 15 K compares favorably with the experimental ZFS values for tetrahedral Co(II). Because of higher magnetic interactions, deviations (lower χ) for **2** start at higher temperatures, about 100 K (Figures 4 and 5). In this case, the deviations below 100 K may come entirely from pretransitional fluctuations that we discuss below. Compound **2** then undergoes a transition at $T_c = 21$ K as indicated by the peak in the ac in-phase susceptibility curve (Figure 5). At the same time, the dc susceptibilities increase rapidly and then reach maximums of values that depend on the direction of the applied field and are consistent with a canted antiferromagnetic state provided that the net moment has components both along the *c*-axis and within the *ac*-plane.

Additional insights into the low-temperature magnetic state of **2** were obtained by recording isothermal magnetization scans that were immediately followed by M vs H loops measured at fields between −50 and +50 kOe. After every loop at a temperature below T_c, the sample was heated up to the paramagnetic state and then zero-field cooled to the next selected temperature. These measurements were made on the partially oriented samples of single crystals. Figure 6 shows the first isothermal ($T = 5$, 12, 18, and 40 K) $M-H$ curves up to 8 kOe. Above the transition temperature at 40 K, only the anticipated linear paramagnetic response is observed. At 18 and 12 K, the curves have the form typical for an antiferromagnet with a weak ferromagnetic moment for both directions of H. The curves start at $M = H = 0$. As H increases, there is an immediate increase in M that resembles that of systems with spontaneous magnetization starting from a domain structure with $M = 0$. Once the saturation of the weak ferromagnetic moment has been reached, the magnetization follows the straight line $M = M_o + \chi H$ up to $H = 50$ kOe, where M_o is the weak ferromagnetic component and χ is the susceptibility of the antiferromagnetic state. The magnetization curves at $T = 5$ K are distinguished by slow initial increases of M, and a threshold field of about 250 Oe is observed for H applied parallel to the *ac*-plane. Table 8 lists values of M_o estimated by extrapolation from large magnetic fields. The ferromagnetic components are quasi temperature-independent between 5 and 18 K, and those measured with H parallel to the *ac*-plane are higher than those measured with H parallel to the *b*-axis. The hysteresis loops at $T = 5$, 12, and 18 K are shown in Figures 7−9, and the estimated remanent moments and coercitive fields are given in Table 8. While there are only small remanent and coercitive

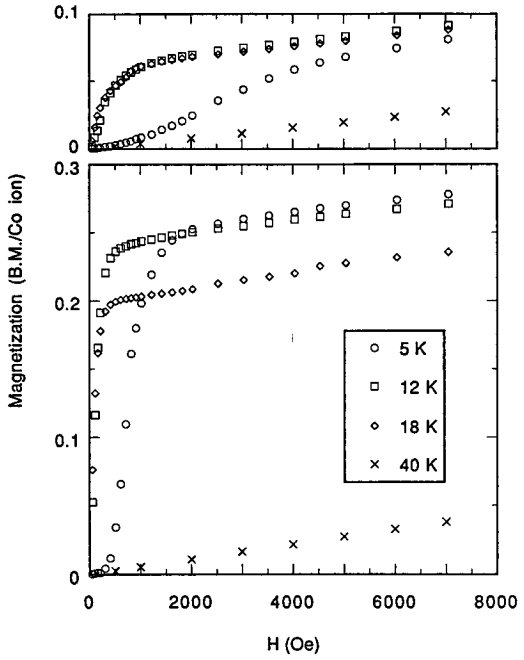

Figure 6. First isothermal magnetization plots of $BaCo_2Si_2O_7$ at $T =$ 5, 12, 18, and 40 K for *H* parallel to the *b*-axis (top) or to the *ac*-plane (bottom).

Table 8. Estimated Values of the Saturated Weak Ferromagnetic Moments (M_o), Remanent Moments (M_r), and Coercitive Fields (H_c) for $BaCo_2Si_2O_7$ at $T = 5$, 12, and 18 K ($T_c = 21$ K)

T (K)	M_o (μ_B/Co ion)	M_r (μ_B/Co ion)	$\lvert Hc\rvert$ (Oe)
	H||*b*		
5	0.06	≅0.035	≅2000
12	0.06	≅0	≅0
18	0.06	≅0	≅0
	H ||*ac*		
5	0.26	≅0.22	≅1000
12	0.25	≅0.12	≅75
18	0.21	≅0.03	≅20

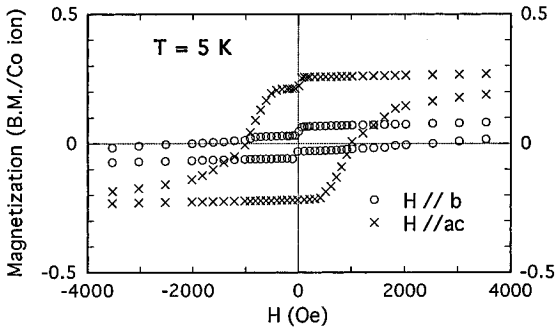

Figure 7. Hysteresis $M-H$ cycles of $BaCo_2Si_2O_7$ at $T = 5$ K for *H* parallel to the *b*-axis or to the *ac*-plane.

(20) Gerloch, M.; Lewis, J.; Rickards, R. *J. Chem. Soc., Dalton Trans.* **1972**, 980.

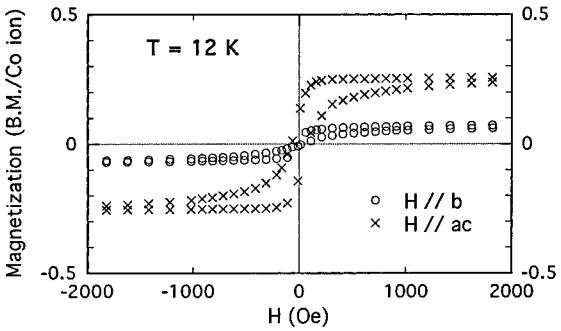

Figure 8. Hysteresis $M-H$ cycles of $BaCo_2Si_2O_7$ at $T = 12$ K for H parallel to the *b*-axis or to the *ac*-plane.

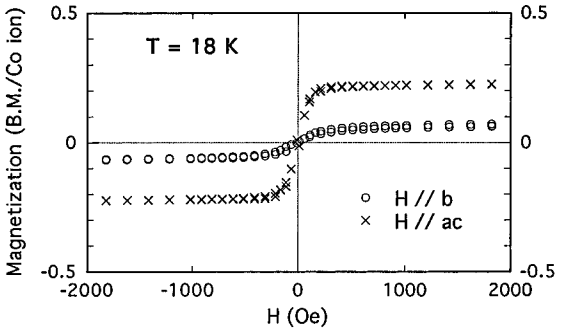

Figure 9. Hysteresis $M-H$ cycles of $BaCo_2Si_2O_7$ at $T = 18$ K for H parallel to the *b*-axis or to the *ac*-plane.

effects at 12 and 18 K, the hysteresis effects at 5 K are quite noticeable with coercitive field values of $|H_c| = 1$ and 2 kOe for H parallel to the *b*-axis and to the *ac*-plane, respectively. Futhermore, the loops at 5 K show well-defined magnetization jumps (Figure 7). Similar jumps have been observed in other antiferromagnets that exhibit a net moment, and it has been suggested that the jumps are due to abrupt changes in the domain structure, *e.g.* abrupt domain-wall motion.[21] These abrupt domain-wall motions are analogous to the Barkhausen jumps observed for ferromagnets.[22]

The behavior of **2** can be explained by a weak ferromagnetism due to spin canting that exists even when no external magnetic field is present. There are two mechanisms for spontaneous spin canting in insulating antiferromagnets.[23−25] One is the antisymmetric Dzyaloshinsky−Moriya (D−M) interaction that results from the anisotropic superexchange interaction; the other is the single-ion anisotropy. Both mechanisms are symmetry-allowed in **2** since two neighboring Co(II) ions are not related by a center of inversion (note that it is not the case for **1**). For a D−M interaction, the spontaneous moment scales with $(\delta g/g)$, where g is the gyromagnetic ratio and δg is its deviation from the free electron value.[25] In other words, the more anisotropic the system, the more important canting will be. The required anisotropy for a D−M interaction to exist is obviously present in **2**. It is also plausible that the single-ion mechanism occurs because the CoO_4 chains are formed from three kinds of tetrahedra that are tilted with respect to each other (see Tables 5 and 6 and Figure 3). It is thus conceivable that the directions of the local easy axis on the Co(II) sites differ from each other. The canting angle can be estimated from the saturated weak ferromagnetic moment M_o observed for $H||ac$ by means of the simple relation $\sin(\gamma) = M_o/gS\mu B$. Thus, at 5 K with $M_o = 0.26\ \mu_B$ (see Table 6), taking $g = 2.0$ and $S = {}^3/_2$, we obtain $\gamma = 5°$.

If **2** was a three-dimensional magnet, we would expect that the paramagnetic susceptibilities will show positive deviations from the modified Curie−Weiss behaviors whatever the spin-canting mechanism.[26] However, in fact, we observe negative deviations, except of course at T_c where the susceptibilites should diverge (see Figures 4 and 5). A low dimensionality of the magnetic lattice can explain this outward discrepancy. In effect, it is well-known that a low-dimensional antiferromagnet should exhibit a broad maximum in its temperature-dependent susceptibility whatever the spin dimensionality, *i.e.* the anisotropy.[27,28] In real 1D systems, this broad maximum often precedes the onset of long-range order induced by interchain coupling. We believe that the paramagnetic susceptibilites of **2** below 100 K have contributions due to both weak ferromagnetism (positive deviations) and low-dimensional short-range spin−spin correlations (negative deviations). The spin canting probably prevents the susceptibility maximums from occuring in **2**, and makes it very difficult to estimate a value of intrachain interactions from the existing numerical work available for 1D antiferromagnets.

Apart from the problems of spin canting and magnetic dimensionalities, it is useful to compare compounds **1** and **2** to other tetrahedral Co(II) compounds. Carlin pointed out some of the features common to tetrahedral Co(II) compounds.[18,19] First, it appears that the magnetic interactions are weak so the compounds are found to order at very low temperatures, below 1 K. Second, the ZFS values, *i.e.* the energy separations between the two spin-doublets of the $^4A_2$ ground terms, are large, on the order of 10−15 K. Hence, for temperatures smaller than the ZFS, one observes Ising or *xy* paramagnetic behaviors with effective spins $S' = {}^1/_2$.[18,19,29] While **1** may behave as generally observed, compound **2** can be said to be very unusual. Compound **2** could represent the first example with the transition temperature ($T_c = 21$ K) being higher than the ZFS and probably orders as a system with real $S = {}^3/_2$ spins.[18,19] One question which must be considered is whether the ZFS affects the magnetic behavior below T_c. As a matter of fact, we observed striking differences in the isothermal behavior of M vs H at 5 K compared to those at 12 and 18 K (see Figures 6−9 and Table 8). Although it is not uncommon for the coercitive field and the remanent moment to increase as the temperature is lowered, the strong increase of the $M-H$ hysteresis between 5 and 12 K is remarkable. The same stands for the work required to saturate the ferromagnetic components (see Figure 6). From a phenomenological point a view, these features could be explained by an increase of the magnetic anisotropy as the temperature decreases from 12 K.[22] A ZFS on the order of 10−15 K may be responsible for this. Anyhow, since ZFS appears as a key for understanding the properties of tetrahedral Co(II), we attempted to measure the ZFS in both compounds using electron paramagnetic resonance (EPR), but no signal could be detected between room temperature and 100 K. However, because of rapid spin−lattice relaxation, the EPR absorption of tetrahedral Co(II) is very often too broad to be detected even at liquid-nitrogen temperature.[13,14]

Supporting Information Available: Tables of data collection parameters and anisotropic thermal parameters for both of the structural analyses (4 pages). Ordering information is given on any current masthead page.

IC960167M

(21) Paduan-Filho, A.; Becerra, C. C.; Barbeta, V. B.; Shapira, Y.; Campo, J.; Palicio, F. *J. Magn. Magn. Mater.* **1995**, *140*−144, 1925.
(22) Chikazumi, S. *Physics of Magnetism*; Krieger Publishing Co.: New York, 1978.
(23) Dzyaloshinsky, I. *J. Phys. Chem. Solids* **1958**, *4*, 241.
(24) Moriya, T. *Phys. Rev.* **1960**, *117*, 635.
(25) Moriya, T. *Phys. Rev.* **1960**, *120*, 91.
(26) Moriya, T. In *Magnetism*; Rado, G. T., Suhl. J., Eds.; Academic Press: New York, 1963; Vol. I.
(27) de Jongh, L. J.; Miedema, A. R. *Adv. Phys.* **1974**, *23*, 1.
(28) Steiner, M.; Villain, J.; Windsor, C. G. *Adv. Phys.* **1976**, *25*, 87.
(29) Carlin, R. L. *J. Appl. Phys.* **1981**, *52*, 1993.